JACS
JOURNAL OF THE AMERICAN CHEMICAL SOCIETY
Article
pubs.acs.org/JACS

A Comprehensive Study of Extended Tetrathiafulvalene Cruciform Molecules for Molecular Electronics: Synthesis and Electrical Transport Measurements

Christian R. Parker,[†] Edmund Leary,*[,‡,§] Riccardo Frisenda,[⊥] Zhongming Wei,*[,†,∥] Karsten S. Jennum,[†] Emil Glibstrup,[†] Peter Bæch Abrahamsen,[†] Marco Santella,[†,∥] Mikkel A. Christensen,[†] Eduardo Antonio Della Pia,[†] Tao Li,[†] Maria Teresa Gonzalez,[§] Xingbin Jiang,[#] Thorbjørn J. Morsing,[†] Gabino Rubio-Bollinger,[‡] Bo W. Laursen,[†] Kasper Nørgaard,[†] Herre van der Zant,*[,⊥] Nicolas Agrait,[‡,§] and Mogens Brøndsted Nielsen*[,†]

[†]Department of Chemistry & Center for Exploitation of Solar Energy & Nano-Science Center & Danish-Chinese Center for Nano-Electronics, University of Copenhagen, Universitetsparken 5, DK-2100 Copenhagen Ø, Denmark

[‡]Laboratorio de Bajas Temperaturas, Departamento de Física de la Materia Condensada Módulo 3, Universidad Autónoma de Madrid, E-28049, Madrid, Spain

[§]IMDEA-Nanoscience, Campus de Cantoblanco, Calle Faraday 9, Ciudad Universitaria de Cantoblanco, E-28049 Madrid, Spain

[⊥]Kavli Institute of Nanoscience, Delft University of Technology, 2600 GA Delft, The Netherlands

[∥]Sino-Danish Centre for Education and Research (SDC), Niels Jensens Vej 2, DK-8000 Aarhus C, Denmark

[#]National Center for Nanoscience and Technology, Beijing 100190, P. R. China

Supporting Information

ABSTRACT: Cruciform-like molecules with two orthogonally placed π-conjugated systems have in recent years attracted significant interest for their potential use as molecular wires in molecular electronics. Here we present synthetic protocols for a large selection of cruciform molecules based on oligo(phenyleneethynylene) (OPE) and tetrathiafulvalene (TTF) scaffolds, end-capped with acetyl-protected thiolates as electrode anchoring groups. The molecules were subjected to a comprehensive study of their conducting properties as well as their photophysical and electrochemical properties in solution. The complex nature of the molecules and their possible binding in different configurations in junctions called for different techniques of conductance measurements: (1) conducting-probe atomic force microscopy (CP-AFM) measurements on self-assembled monolayers (SAMs), (2) mechanically controlled break-junction (MCBJ) measurements, and (3) scanning tunneling microscopy break-junction (STM-BJ) measurements. The CP-AFM measurements showed structure−property relationships from SAMs of series of OPE3 and OPE5 cruciform molecules; the conductance of the SAM increased with the number of dithiafulvene (DTF) units (0, 1, 2) along the wire, and it increased when substituting two arylethynyl end groups of the OPE3 backbone with two DTF units. The MCBJ and STM-BJ studies on single molecules both showed that DTFs decreased the junction formation probability, but, in contrast, no significant influence on the single-molecule conductance was observed. We suggest that the origins of the difference between SAM and single-molecule measurements lie in the nature of the molecule−electrode interface as well as in effects arising from molecular packing in the SAMs. This comprehensive study shows that for complex molecules care should be taken when directly comparing single-molecule measurements and measurements of SAMs and solid-state devices thereof.

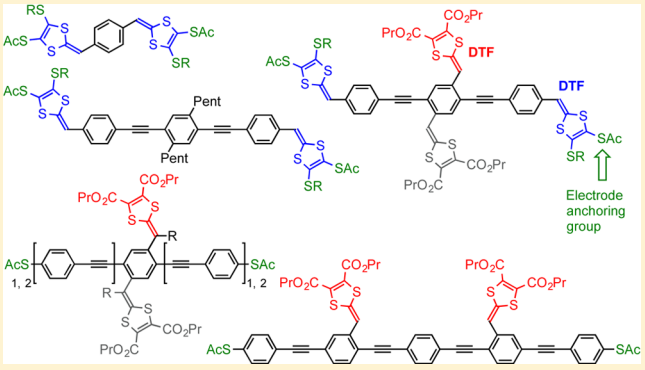

INTRODUCTION

Development of organic molecules as components for molecular electronics devices has attracted interest as a means of achieving miniaturization of integrated electronic circuits.[1] In particular, nanometer-sized π-conjugated molecules are suitable as wires owing to their delocalized electrons and small HOMO−LUMO gaps. Detailed investigations of molecular conductivity as a function of molecular structure and molecule-electrode anchoring groups are particularly important for the

Received: June 6, 2014
Published: November 6, 2014

   dx.doi.org/10.1021/ja509937k | J. Am. Chem. Soc. 2014, 136, 16497−16507

development of the field. Such structure−property relationships have been established from studies of single-molecule junctions and self-assembled monolayers (SAMs), and they reveal that the molecular conductance depends on several parameters such as molecular length, HOMO−LUMO gap, molecular geometry, quantum interference phenomena, and the nature and positions of anchoring groups.[1,2]

Tetrathiafulvalene (TTF) has played a key role in molecular electronics since Aviram and Ratner[3] in 1974 suggested that a molecular rectifier could be obtained by linking together this donor and the electron-acceptor tetracyanoquinodimethane via a nonconjugated bridge. Thus, several TTF-based intramolecular charge-transfer compounds have been prepared and some tested in junctions.[4] Owing to the three redox states of TTF (0, +1, +2), several TTF-based wires, switches, and memory devices have also been prepared.[5] Oligo(phenyleneethynylene)s (OPEs) present another class of π-conjugated molecules employed as wires.[2] Thiols/thiolates, conveniently protected as thioacetates, are often used for anchoring such molecules to metal electrodes,[6] but also alkylsulfides and disulfides act as anchoring groups at metal surfaces/junctions.[6,7]

We have in recent years combined OPEs and TTF in cruciform-like structures in which dithiafulvenes (DTFs) are placed perpendicularly to an OPE backbone, hence incorporating an extended TTF (exTTF).[8] π-Conjugated cruciform motifs have in general attracted interest for their electronic and optical properties.[9] Acetylenic benzene-extended TTF building blocks were developed which allowed for stepwise construction of OPE-TTF cruciforms.[8a−d,f] An enhanced stability of these modules relative to other acetylenic motifs[10] presented a major advantage. Previously, conducting probe (CP) atomic force microscopy (AFM) measurements on SAMs on gold of two cruciform molecules with thioacetate anchoring groups revealed an increased conductance relative to simple OPEs.[8c] Moreover, we have contacted an OPE5-TTF cruciform in a three-terminal geometry and showed gate-controlled conductance switching.[8e] In 2013 we reported a new class of exTTF cruciforms in which SAc-functionalized DTFs were incorporated as termini.[8d,f] These molecules are composed of two perpendicularly oriented exTTFs. The DTF-thiolate anchoring groups seemed to form stable, highly conducting molecular junctions in break-junction experiments. Yet, significantly lower conductances were obtained by CP-AFM measurements on SAMs. To elucidate in detail how the charge-transport properties are influenced by the molecular structure, anchoring groups, and the experimental technique, we designed a large selection of cruciform motifs in which the number and placement of DTF units along an OPE is systematically changed.

The target molecules (and reference molecules) can be divided into six classes (Chart 1). Class [*x*.*y*] corresponds to molecules with *x* DTFs as termini of the OPE and *y* DTFs placed orthogonally to the OPE. Class [0.0] with no DTFs is represented by the simple OPE3 and OPE5 wires **1**[2a] and **2**,[8c] while class [0.1] in total has one DTF unit, placed along the wire (OPE3s **3**, **4**, and OPE5 **5**). Molecules with one additional DTF along the OPE ([0.2]) are represented by OPE3s **6**−**9** and OPE5s **10** and **11**. We have previously described the syntheses of OPE3-bisDTFs **6**[8a,b] and **8**[8d] and of the OPE5-bisDTF 10.[8b] We found that **8** containing no SAc end groups showed no binding in break junctions, nor did it form SAMs on gold. To explore the influence of distortion of the π-system from planarity, we designed OPE3 **9** with Me groups at the

Chart 1. Cruciforms Classified by Number of DTFs along the OPE (in red) and As Termini (in blue)

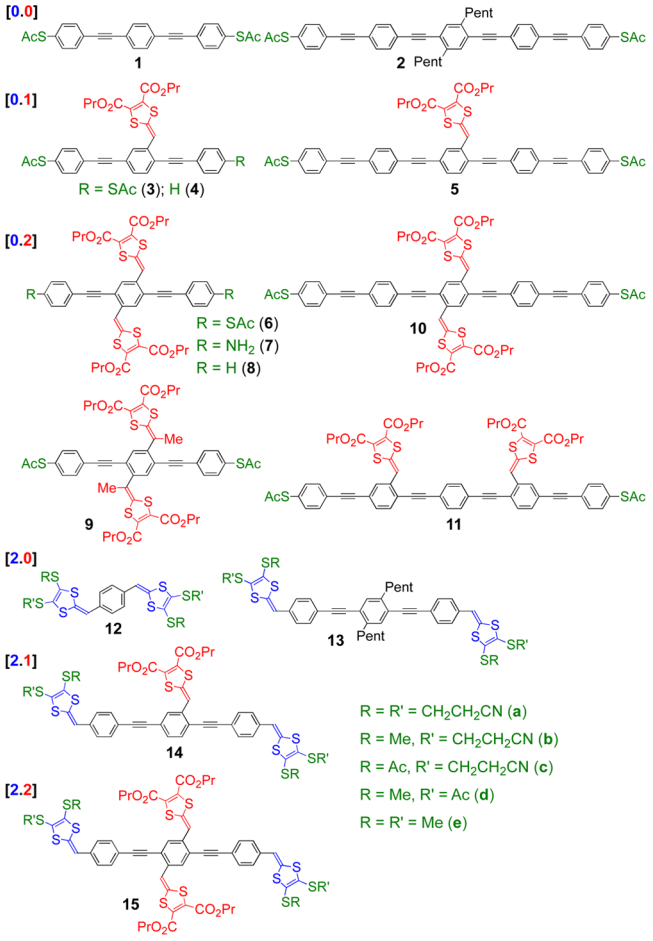

exocyclic fulvene C atoms. Compounds **12** and **13** only have DTFs as termini, one at each end of the wire ([2.0]). Compounds **14** ([2.1]) and **15** ([2.2]) have DTF termini and, in addition, one and two DTFs, respectively, along the wire. Compounds **12**−**15** have different substitution patterns of the DTF termini (SCH_2CH_2CN, SMe, SAc). Synthesis and studies of compounds of structure **15** build upon a recent communication.[8d] Conductance studies were performed using (1) CP-AFM measurements on SAMs, (2) mechanically controlled break-junction (MCBJ) experiments on single molecules, and (3) scanning tunneling microscopy break-junction (STM-BJ) experiments on single molecules.

RESULTS AND DISCUSSION

Synthesis. The DTF unit is in general introduced from suitably alkyne-functionalized derivatives of benzaldehyde in a Wittig reaction. Chart 2 shows suitable building blocks (**16**−**19**) for the preparation of OPE-DTFs, that is, OPEs with one DTF group. The synthesis of **16**, **18**, and **19**, provided in Supporting Information (SI), starts out from triflation of 2,5-

Chart 2. Arene Building Blocks

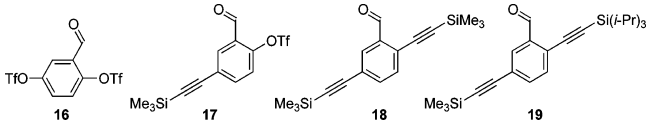

dx.doi.org/10.1021/ja509937k | J. Am. Chem. Soc. 2014, 136, 16497−16507

Scheme 1. Synthesis of OPE3-DTFs and OPE5-DTF ([0.1]) (Pr = *n*-Pr)

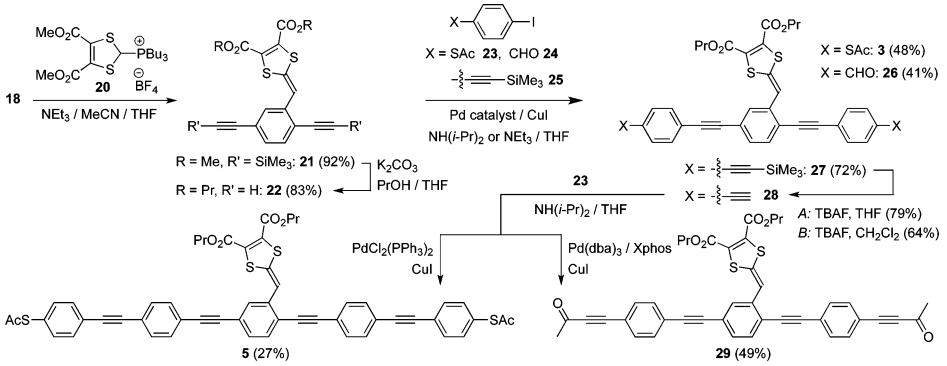

dihydroxybenzaldehyde followed by Sonogashira cross-coupling[11] reactions with suitable alkynes. The corresponding CO_2Me derivatives[12,13] (instead of CHO) of **16** and **18** can also be used as precursors as the CO_2Me group is readily converted to the desired aldehyde functionality by a reduction followed by oxidation protocol (see SI). For synthesis of **17**, we refer to Wang et al.,[14] and for an alternative route to **18**, we refer to Cade et al.[15]

With compound **18** in hand, the OPE3-DTF **3** and OPE5-DTF **5** can be prepared according to Scheme 1. First, **18** was treated with the phosphorus ylide generated from the known phosphonium salt **20**,[16] affording the DTF compound **21**. Desilylation accompanied by transesterification, enhancing solubility (CO_2Me to CO_2Pr, Pr corresponds to *n*-Pr everywhere), gave the product **22**, which was treated with either **23**,[8b] **24**, or **25** under Sonogashira conditions to furnish OPE3s **3**, **26**, and **27**. Desilylation of **27** to **28** followed by a coupling with **23** using the $PdCl_2(PPh_3)_2$/CuI catalyst system gave the SAc end-capped OPE5-DTF **5**. To our surprise, changing the catalyst system to $Pd(dba)_3$/Xphos/CuI gave the product **29**, resulting from acetylation of the acetylides. While acetylation reactions to our knowledge have not been effected by this specific catalyst system, they were reported under other catalyst conditions.[17] An alternative protocol for constructing the OPE3-DTF core is shown in Scheme 2. Here the core was

Scheme 2. Synthesis of OPE3-DTF ([0.1]) with *tert*-Butyl-Protected Thiol End Groups

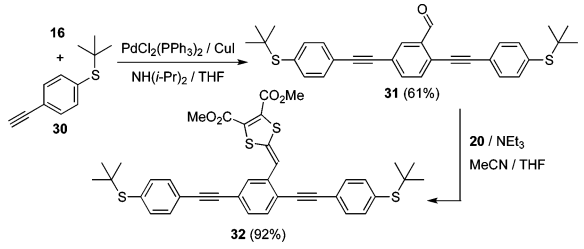

first prepared by treating the ditriflate **16** with the known alkyne **30**.[6b] The product **31** was subjected to a Wittig reaction with **20** affording the OPE3-DTF **32** with *tert*-butylthio end groups. Such groups can be converted to thioacetates in the presence of DTF units[8a] and can also be used directly as electrode anchoring groups (when weak binding is preferred).[7c]

The unsymmetrical OPE3-DTF **4** was prepared according to Scheme 3. Compound **17** has both an aldehyde and a triflate functionality, which allows it to be either subjected to a Wittig reaction, affording the DTF compound **33**, or a Pd-catalyzed

Scheme 3. Synthesis of Asymmetrical OPE3-DTF ([0.1]) with Only One SAc End Group

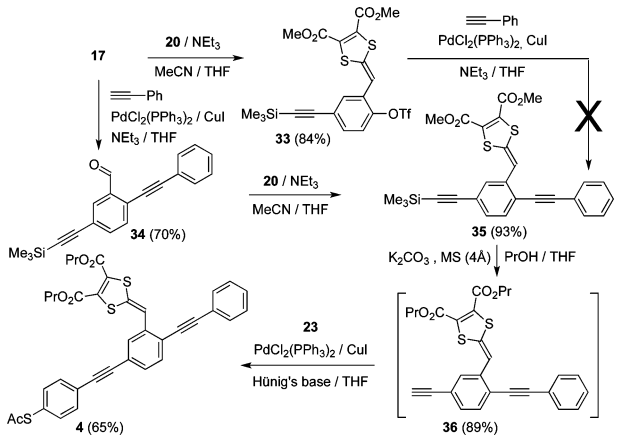

coupling with phenylacetylene, affording the OPE2 derivative **34**. While we were not able to convert **33** to the OPE2-DTF **35**, compound **34** was successfully converted to **35**. Finally, desilylation followed by cross-coupling between the intermediate (**36**) and **23** gave **4**.

The OPE3-bisDTF **7** with NH_2 end groups was prepared according to Scheme 4. First the known conversion of **37** to **38**

Scheme 4. Synthesis of OPE3-bisDTF ([0.2]) with NH_2 End Groups

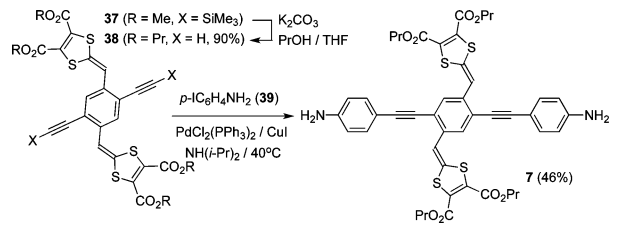

was performed;[8b] **38** was then coupled with *p*-iodoaniline (**39**), giving target molecule **7**. We also prepared the related Boc-protected derivative of **7** from the Boc-protected *p*-iodoaniline[18] (see SI), but attempts of removing the Boc groups afterward were, however, not successful. Instead we isolated a compound, which from spectroscopic and mass data seemed to be the product where HCl had added to each of the fulvenes.

Synthesis of OPE3-bisDTF **9** is shown in Scheme 5. First, the known dialdehyde **40**[8a] was treated with MeMgBr, and the resulting alcohol (mixture of stereoisomers, used crude) was

dx.doi.org/10.1021/ja509937k | J. Am. Chem. Soc. 2014, 136, 16497−16507

Scheme 5. Synthesis of OPE3-bisDTF ([0.2]) with Methyl Substituents at the Fulvene Units

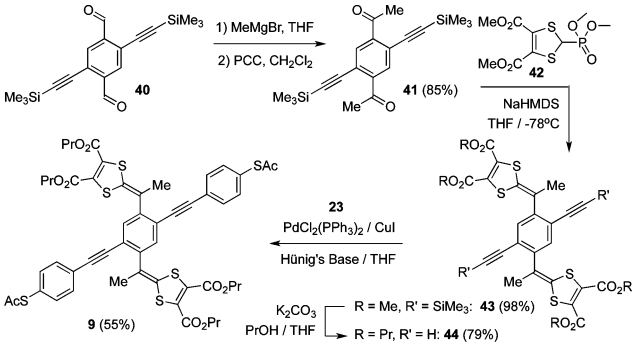

oxidized by PCC. The diketone **41** was treated with the phosphonate ester **42**,[19] deprotonated by NaHMDS, to afford the product **43** in a Horner–Wadsworth–Emmons reaction.[20] The structure was confirmed by X-ray crystallographic analysis (Figure 1),[21] which showed the two DTFs to be almost

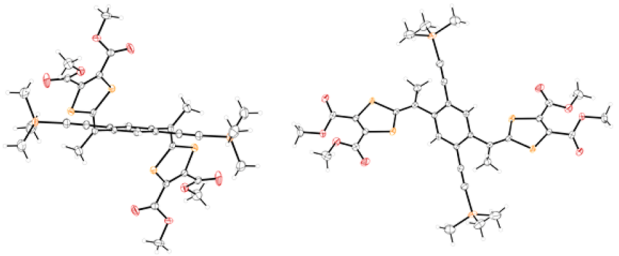

Figure 1. ORTEP plots showing molecular structure of **43** (two views).

perpendicular to the plane of the central benzene ring, in contrast to the planar structures of **37**[8a] and **8**.[8d] Desilylation/transesterification followed by coupling with **23** finally gave **9**.

Incorporation of two DTFs along an OPE5 at two different benzene rings was performed according to Scheme 6. First, **19** was subjected to a Wittig reaction to form the DTF compound **45**, which was then subjected to a sequence of desilylation (and transesterification) and Sonogashira reactions to ultimately give **11**.

The next objective was to prepare molecular wires with DTF termini. Phosphite-mediated coupling between benzaldehyde derivatives and 4,5-dialkylthio-1,3-dithiole-2-thiones was previously shown to provide an efficient route to phenyl-DTFs.[8f] Mulla and Zhao[22] have also recently used this strategy for incorporating DTFs as termini of OPEs. Heating terephthaladehyde **50** and thiones **51a**[23] and **51b**[24] in $P(OEt)_3$ gave exTTFs **12a** and **12b** (Scheme 7); we previously used the same method to prepare **12e** (from **50** and **51e**).[8f] Removal of one

Scheme 7. Synthesis of Extended TTFs ([2.0])

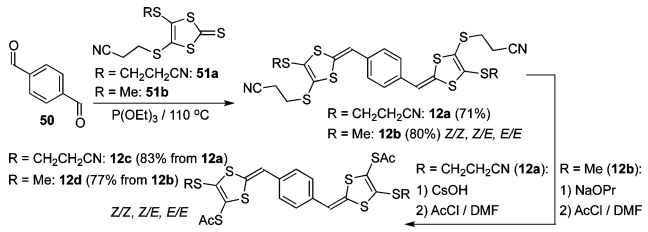

cyanoethyl group at each DTF by treatment with CsOH generated dithiolates, which were acetylated to give products **12c** and **12d**.

OPE3s **13**–**15** with DTF termini were made by a combination of phosphite-mediated couplings and Sonogashira reactions, recently used to prepare derivatives **15a**–**d**.[8d,f] The aryl iodides **52a,b,e** (Scheme 8) are key building blocks for the

Scheme 8. Synthesis of OPE3s with DTF Termini ([2.0], [2.1], [2.2])[a]

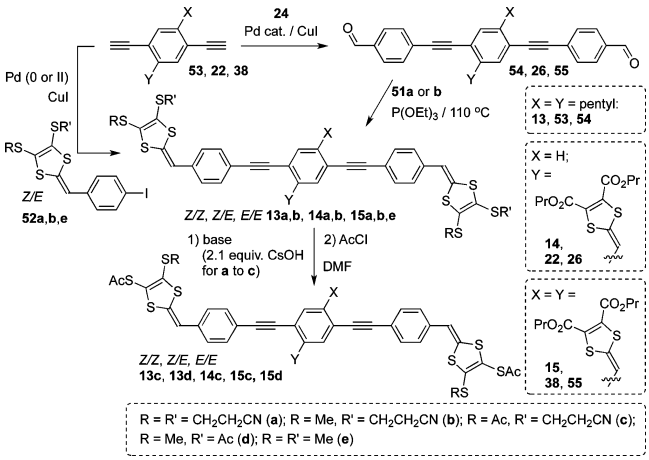

[a]Yields/conditions: Table 1.

Sonogashira reactions. Compound **52a** was previously prepared from 4-iodobenzaldehyde and 4,5-bis(2′-cyanoethylthio)-1,3-dithiole-2-thione using $P(OEt)_3$.[8f] Cyanoethyl deprotections followed by methylation/acetylation of the intermediate thiolates gave methylated and acetylated derivatives (see SI). Synthesis of the rather unstable alkyne coupling partner **53**, incorporating solubilizing pentyl groups, is shown in SI. From these key building blocks, together with the diynes **22** and **38**

Scheme 6. Synthesis of OPE5-bisDTF ([0.2])

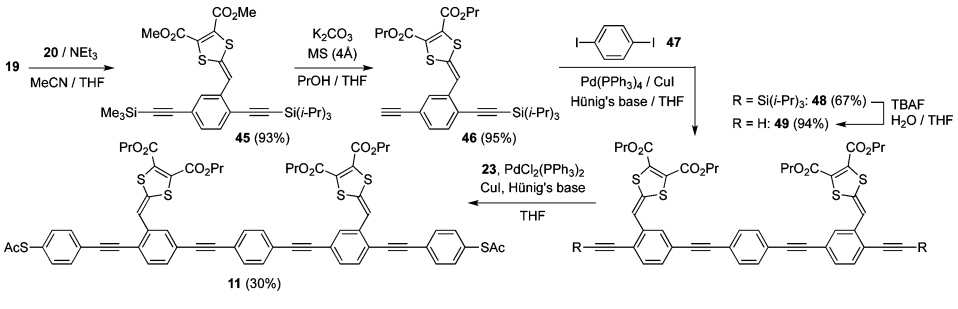

dx.doi.org/10.1021/ja509937k | J. Am. Chem. Soc. 2014, 136, 16497–16507

and *p*-iodobenzaldehyde (**24**), differently substituted derivatives of **13**−**15** were prepared according to Scheme 8 and Table 1. Different stereoisomers were obtained for DTFs containing two different substituents (*Z*/*E*).

Table 1. Conditions and Yields for Scheme 8

entry	starting material(s)	conditions	product	yield
1	**53** + **52a**	$PdCl_2(PPh_3)_2$/CuI; NEt_3[a]	**13a**	11%
2	**54** + **51a**	$P(OEt)_3$; 110 °C	**13a**	80%
3	**53** + **52b**	$Pd(OAc)_2$/CuI/dppf/PPh_3; NEt_3/PhMe; sonication 45 °C	**13b**	50%
4	**26** + **51a**	$P(OEt)_3$; 110 °C	**14a**	81%
5	**26** + **51b**	$P(OEt)_3$; 110 °C	**14b**	37%
6	**55** + **51a**	$P(OEt)_3$; 110 °C	**15a**	72%[b]
7	**38** + **52b**	$Pd(PPh_3)_4$/CuI; NH(*i*-Pr)$_2$	**15b**	54%
8	**55** + **51b**	$P(OEt)_3$; 100 °C	**15b**	66%
9	**38** + **52e**	$PdCl_2(PPh_3)_2$/CuI; THF/NEt_3; sonication 40 °C	**15e**	54%
10	**13a**	CsOH; AcCl; DMF/PrOH	**13c**	36%
11	**13b**	KO*t*-Bu; AcCl; DMF	**13d**	64%
12	**14a**	CsOH; AcCl; DMF/PrOH	**14c**	68%
13[c]	**15a**	CsOH; MeI; DMF/PrOH	**15b**	87%
14[c]	**15a**	CsOH; AcCl; DMF/PrOH	**15c**	53%
15[c]	**15b**	CsOH; AcCl; DMF/PrOH	**15d**	19%

[a]Initially: NH(*i*-Pr)$_2$/THF. [b]A yield of 63% was previously reported under similar conditions; ref 8d. [c]Ref 8d.

We have previously[8d] reported synthesis of **15a** by a phosphite coupling and converted this compound to either **15b** or **15c**; the former could subsequently be converted to **15d**. Scheme 8 shows a more direct route to **15b** by incorporating the DTF termini from the precursor **38**. Compounds **13a**,**b** and **14a**,**b** can also be synthesized by two other methods, starting from bis-terminal alkynes **53**, **22**, and **38**, which in the first method (Table 1, entries 1, 3, 7, 9) were coupled with DTF-functionalized iodobenzene (**52a**,**b**,**e**). This coupling was quite slow and only gave poor to moderate yields (11−54%) and a number of byproducts. We tried to couple the thioacetate **52d** with **38** aiming at a direct synthesis of **15d**, but the reaction did not go to completion and gave several byproducts. A more successful method coupled *p*-iodobenzaldehyde **24** to the alkynes **53**, **22**, and **38**; these reactions were noticeably faster when the amine was used as neat solvent. Dialdehydes **54**, **26**, and **55** were then coupled with thiones **51a**,**b** using $P(OEt)_3$ (Table 1, entries 2, 4−6, 8) to give products in 70−80% yields.

As for **12a**, removal of one cyanoethyl group on each DTF in **13**−**15a** was achieved by CsOH. While methylation of the intermediate thiolate worked in high yield (87%; entry 13), yields were generally low for acetylations (19−68%; entries 10−12, 14, 15). With a large excess of AcCl, the desired product was not obtained. For **14** and **15** with central DTFs, a reaction with HCl seemed to occur. Finally, we note that attempts of preparing derivatives of **15** and **52** with two SAc groups at each DTF were not successful; only unstable products were obtained.

UV−vis Absorption and Fluorescence Spectroscopy. The optical properties were studied in CH_2Cl_2 (all data are included in SI). Addition of DTFs along the OPE results in a new red-shifted longest-wavelength absorption band as revealed by comparing OPE3s **1** [0.0], **3** [0.1], and **6** [0.2] (Figure 2) (and from OPE3s **13a** [2.0], **14a** [2.1], and **15a** [2.2], see SI).

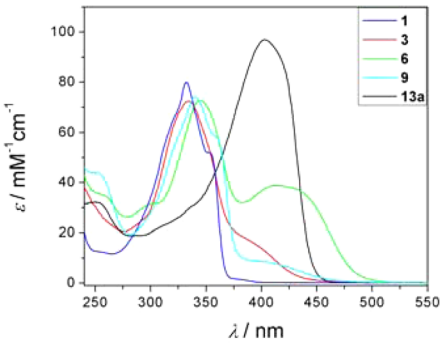

Figure 2. UV−vis absorption spectra of **1** [0.0], **3** [0.1], **6** [0.2], **9** [0.2], and **13a** [2.0] in CH_2Cl_2.

The broken conjugation in nonplanar **9** [0.2] causes a blueshift in the end-absorption relative to that of **6**. Comparison of OPE3s **6** [0.2] and **13a** [2.0] shows that having two DTFs along the OPE induces a larger redshift than two DTF termini. OPE5 **10** [0.2] exhibits a longest-wavelength absorption maximum (427 nm) red-shifted relative to that of **11** (360 nm), with DTFs at different benzene rings.

The photoluminescence spectra showed broad and unresolved bands, and the emission peaks are red-shifted for the OPE-DTFs (SI). The DTF unit also causes the compounds to be only weakly fluorescent relative to the parent OPEs **1** and **2**. Fluorescence quenching was recently reported for other DTF-end-capped OPE/OPV oligomers.[22]

Electrochemistry. The redox properties of representative compounds were studied by cyclic voltammetry and differential pulse voltammetry at concentrations of ca. 1 mM in CH_2Cl_2 + 0.1 M Bu_4NPF_6 (data listed in SI). Most of the compounds were oxidized irreversibly at a scan rate of 100 mV/s, as previously seen for DTF compounds due to radical dimerization.[25] At higher scan rates (1 V/s) the reversibility became slightly better for **37**, and two waves were discernible in the forward and backward scans (see SI). By substituting one of the $SiMe_3$ groups of **37** for a Si(*i*-Pr)$_3$, we found previously[8b] partially reversible oxidations at half-wave potentials of 0.56 and 0.67 V vs Fc/Fc^+ at a scan rate of 100 mV/s. The bulky Si(*i*-Pr)$_3$ may help to slow down dimerization, but better reversibility may also be a concentration effect. Thus, for a very dilute sample of **3**, the first oxidation seemed to approach reversibility. More electron-rich DTFs with alkylthio substituents (**12a**, **15a**) were easier to oxidize than DTFs with ester groups (**6**, **8**). ExTTF **43** in which the fulvene H's are replaced by Me's, preventing radical dimerization, exhibited a reversible two-electron oxidation (see SI). This oxidation (E = +0.72 V vs Fc/Fc^+) is significantly anodically shifted (by 0.2 V) relative to that of **37** (E_{pa} = +0.54 V), presumably due to the orthogonal arrangement of the two DTFs, also rendering them independent redox centers.

CP-AFM Measurements on SAMs. High-quality SAMs could be grown on Au substrate of most of the OPEs (dissolved in Et_3N/THF) with SAc end groups through the optimization of growth conditions (following a general protocol).[8c,26] Most of the OPE SAMs were free of pinholes and defects and densely packed with high coverage as checked by electrochemistry. The experimental thickness of the SAMs of OPE3 **1** (1.78 nm), OPE3-DTF **3** (1.96 nm), OPE3-bisDTF **6** (2.36 nm), OPE5 **2** (3.03 nm), and OPE5-bisDTF **10** (3.10 nm) were determined from XPS data. Conductances were measured by CP-AFM in vertical structure junctions. This method was previously shown,

dx.doi.org/10.1021/ja509937k | J. Am. Chem. Soc. 2014, 136, 16497−16507

using a Pt AFM tip, to be efficient for measuring transport properties of SAM-based molecular junctions trapping several hundred molecules.[27] In the present work, a Au-coated conductive tip was used as top electrode forming a Au/SAM/Au vertical junction. The same tip was used for all measurements ensuring a constant contact area in the junctions. This allows for comparison of relative conductance between the different SAMs but not directly with the single-molecule conductance since the actual number of molecules in the junctions is unknown.

The results are collected in Table 2 and averaged $I-V$ curves are shown in SI. The conductance values were the average data

Table 2. CP-AFM Measurements on SAMs

compound	DTFs [$x.y$]	conductance[a] (nS)	average resistance (Ω)
OPE3 **1**	[0.0]	1.49 ± 0.48	6.71×10^8
OPE5 **2**	[0.0]	0.58 ± 0.35	1.72×10^9
OPE3 **3**	[0.1]	2.85 ± 2.23	3.51×10^8
OPE5 **5**	[0.1]	0.76 ± 0.60	1.32×10^9
OPE3 **6**	[0.2]	5.56 ± 2.81	1.80×10^8
OPE3 **9**	[0.2]	3.61 ± 2.75	2.77×10^8
OPE5 **10**	[0.2]	2.28 ± 1.53	4.39×10^8
OPE5 **11**	[0.2]	1.65 ± 0.91	6.06×10^8
"OPE1" **12d**	[2.0]	143.6 ± 91.3	6.96×10^6
"OPE3" **13d**	[2.0]	2.06 ± 1.06	4.85×10^8
"OPE3" **15d**	[2.2]	4.06 ± 1.23	2.46×10^8

[a]Errors are the standard deviation of the mean.

of about 200 measurements and determined over a small bias range of ±0.1 V. We notice that the conductance decreases with the length of the molecules. If the number of DTFs are the same, an OPE5 shows lower conductance than the related OPE3 (OPE5 **10** vs OPE3 **6** and OPE5 **5** vs OPE3 **3**). Previous measurements using a Pt AFM tip showed that the conductance increased (by a factor of ca. 9) when proceeding from OPE3 **1** to OPE3-bisDTF **7** or from OPE5 **2** to OPE5-bisDTF **10**.[8c] Measurements on the large selection of OPE3 and OPE5 molecules support this trend for both series as depicted in Figure 3. For the OPE3 series, we observe that the conductance increases as the number of DTFs along the wire increases. Thus, as indicated by the red arrows, for the OPE3 series the conductance increases in the sequences: **1** [0.0] < **3** [0.1] < **6** [0.2] and **13d** [2.0] < **15d** [2.2]. For the OPE5 series, the same influence of the DTFs is observed: **2** [0.0] < **5** [0.1] < **10** and **11** [0.2]. This behavior indicates that electron transport in the SAMs is dominated by the molecular HOMO, which is raised in energy by DTF units. The OPE5 series also reveals that the position of the DTFs along the wire has an influence; both OPE5 **10** and **11** have two DTFs ([0.2]), but when they are on the same benzene ring in the middle of the backbone (**10**), a higher conductance is obtained. By changing the position of these electron-donating substituents, we make small changes in the HOMO, again supporting this as an important transport channel in these SAM experiments. A strong effect of the DTF termini is also observed; **12d** ("OPE1" [2.0]) exhibits a conductance 2 orders of magnitude larger than the other molecules, although it is of comparable length to the OPE3s (but shows a very broad range in conductance values). Similarly, it is evident that substituting aryl groups in the OPE5s for DTF termini increases the conductance (OPE3 **15d** vs OPE5 **10** and OPE3 **13d** vs OPE5 **2**). The effect of DTF termini within the OPE3 series is more difficult to generalize (blue arrows in Figure 3). Proceeding from OPE3 **1** to **13d** results in an increased conductance although the length of the molecule is increased, while OPE3 **15d** with two DTF termini shows a reduced conductance relative to the shorter OPE3 **6**. The influence of distorting the DTF units from coplanarity is revealed by comparing [0.2] OPE3s **6** and **9**; the conductance of nonplanar **9** is only ca. 65% that of **6**. OPE3 **4** with only one SAc did not form good SAMs (low coverage density), and we could not grow good SAMs of **15e**.

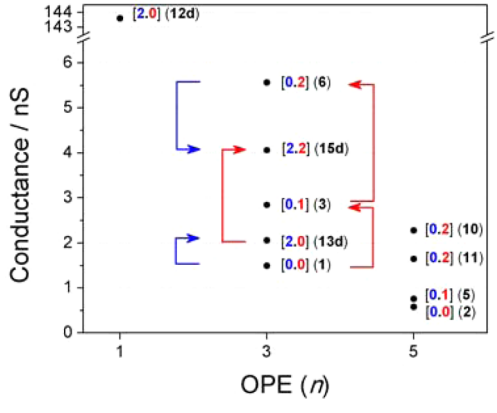

Figure 3. Conductances of SAMs as a function of the OPE length and number and position of DTF units.

Single-Molecule Conductivity Studies. The conductance of **1**, **3**, **6**, **7**, **9**, **10**, and **15c** was measured using the STM-BJ (Madrid) and MCBJ (Delft) methods. For the STM between 5000 and 10000 traces were recorded per compound and 1000−2000 for the MCBJ. Figure 4 shows representative

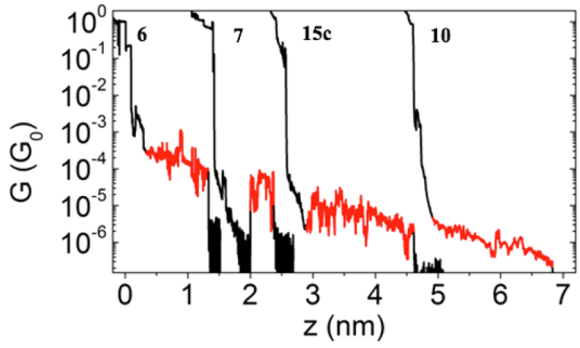

Figure 4. Representative individual G *vs* z traces for molecules **6**, **7**, **15c**, and **10** (more examples in SI) with plateau regions highlighted in red. OPEs **1**, **3**, **6** and **9** show similar plateau profiles to **6**, and only a typical trace of **6** is presented. For **7** the junctions often form after the gold contact rupture. Lower gains were used for the traces of **6** and **7** than for **15c** and **10**, which places the noise level at 10^{-6} G_0 and 10^{-7} G_0, respectively.

conductance vs distance traces ($G(z)$) for **6**, **7**, **15c**, and **10** (STM data). At values close to 1 G_0, small plateaus in G, followed by a sharp drop, indicate the final breakdown of the gold contact. Below this, longer plateaus indicate molecular junction formation, where one or a few molecules may be bound between the electrodes. The plateaus for all compounds generally fluctuate up to 1 order of magnitude from beginning to end, with discrete jumps between different conductance states visible as the junction is elongated. At the end, a sharp drop in current indicates breakdown of the junction. 1D and

dx.doi.org/10.1021/ja509937k | J. Am. Chem. Soc. 2014, 136, 16497−16507

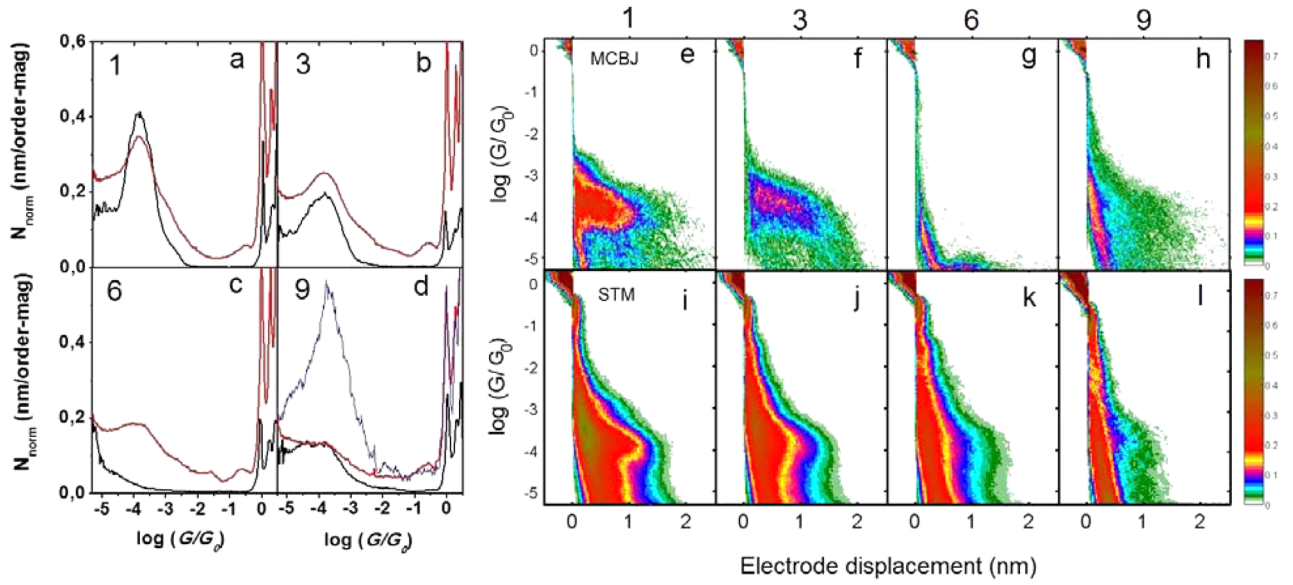

Figure 5. Left: 1D normalized histograms of **1** (a), **3** (b), **6** (c), **9** (d) measured in Madrid (red) and Delft (black) with no data selection. Blue histogram in (d) contains only selected plateaus of **9** (STM) to amplify the low molecular signal. Right: 2D normalized histograms using MCBJ [**1** (e), **3** (f), **6** (g), **9** (h)]; STM [(**1** (i), **3** (j), **6** (k), **9** (l)].

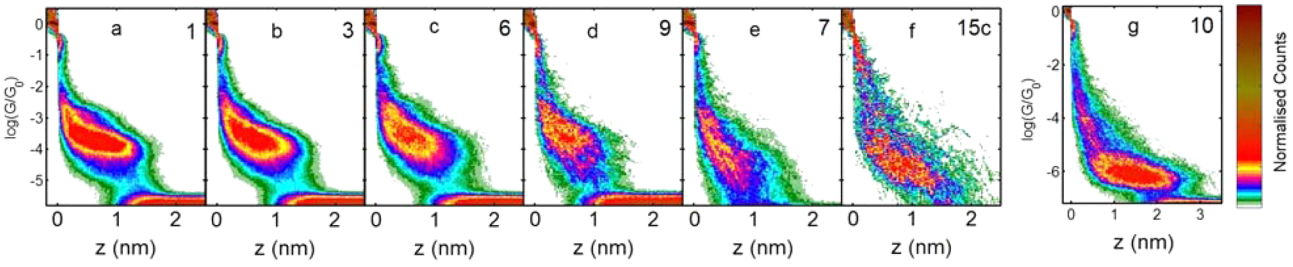

Figure 6. 2D histograms of the traces containing plateaus of **1**, **3**, **6**, **9**, **7**, **15c**, and **10** from the STM-BJ technique. All histograms have been plotted with the same $x-y$ axes, apart from **10** due to the longer plateaus and lower conductance.

2D histograms were built from the total recorded data (Figure 5). We also carried out a selection of only the traces containing plateaus (from STM data), the 2D histograms of which are shown in Figure 6 (see SI for 1D histograms). Figure 5a–d shows the 1D conductance histograms for molecules **1**, **3**, **6**, and **9** without data selection; each bin is equal to log (G/G_0) = 0.02 for the STM data and 0.04 for the MCBJ data. Histograms were normalized according to ref 28.

Comparing the results between the two setups in the two different laboratories, we find that the 1D histograms for molecules **1** and **3** (Figure 5a,b) are generally very similar. The peaks located close to $\log(G/G_0) = -4$ are centered at practically the same values for both molecules in both setups. This value is also very similar to another OPE3 we previously studied containing two hexyloxy substituents on the central benzene ring.[28] The lower peak height of **3** compared to **1** is also reproduced in both setups and is a result of a lower percentage of plateaus obtained for **3** (with the STM we find that 26% of traces show plateaus for **1** and 18% for **3**). The normalized 2D histograms of **1** and **3** from the MCBJ setup are shown in Figure 5e,f and those of the STM in Figure 5i,j. The color scale indicates the number of counts normalized to the number of curves used to build the histograms, and to aid comparison between the two sets of data we use the same range for both. From the STM data, the mean plateau length for **1** and **3** was found to be 1.28 and 1.25 nm, respectively (see SI for plateau length distributions). We generally expect an initial gap of approximately 0.5 nm due to relaxation of one or two gold atoms in the electrodes, putting the mean real interelectrode spacing very close to the S–S distance of **1** and **3** (both 2.07 nm). The 95th percentile values were 1.84 and 1.87 nm, which are only slightly less than the molecular length and represent the few junctions in which the snap-back is very small. The use of this particular color scale also shows that no plateaus were found for **6** with the MCBJ, while a definite signal is obtained by STM, albeit weaker than for **1** and **3**. The percentage of plateaus found for **6** with the STM was 12% in the run shown in Figure 5c. Several samples were measured with the STM, also giving weak signals, and we had to test several different areas to produce the results shown in Figure 5c. Clearly, statistically speaking, this molecule is harder to trap than **1** and **3**, so it is reasonable to assume that in the MCBJ, where only a single pair of electrodes can be used, there is a much smaller probability of wiring than in the STM.

Molecule **9** gives a weak signal in both setups, which is not so clear looking at the 1D histogram (Figure 5d, 9% plateaus). The signal is, however, clearly visible in the 2D histograms thanks to the choice of contrast, which enables low counts to be viewed in blue/green (Figure 5g,k). In order to emphasize the weak signal in the 1D histogram, we have plotted only the selected plateaus from the STM data, which shows that the peak is located in roughly the same position as for **1**, **3**, and **6**.

dx.doi.org/10.1021/ja509937k | J. Am. Chem. Soc. 2014, 136, 16497–16507

Molecule **9** is similar in structure to **6** but has a Me group on each of the DTFs. The fact that a signal is seen for **9** but not for **6** in the MCBJ study may suggest that the Me groups play a role in helping junction formation. In the STM results, however, we find roughly the same percentage of plateaus for both molecules **6** and **9**. As it is hard, however, to control the precise conditions that might influence the junction formation probability on any given sample (especially the distribution of molecules on the surface), we cannot place too much emphasis on the final overall percentage. We suggest that while the number of experimental runs (i.e., number of separate samples prepared) is too low to draw solid conclusions about the efficacy of the additional methyl groups, they may slightly help to form junctions incorporating a TTF unit.

Overall, there seems to be a clear tendency, which is seen in both setups, for the junction formation probability to decrease with the number of DTF side groups (the highest percentages found with the STM method were 26%, 18%, 12% and 9% for molecules **1**, **3**, **6**, and **9**, respectively). This strongly suggests that the DTF groups hinder the formation of junctions, most likely due to their additional S atoms. These can potentially interact with the gold to reduce the mobility of the molecule, which would make it harder for it to diffuse toward the junction. Additionally, this could also make it more difficult to suspend the molecule freely between the contacts. The similarity in the position of the conductance peaks of molecules **1**, **3**, **6**, and **9** shows that there is, however, negligible electronic influence of the DTF units, at least in the low bias regime, with the most probable conductance lying between 1.5 and 1.8 × 10^{-4} G_0 for all molecules. The histograms have a broadness of approximately 1 order of magnitude at half-maximum, which can be explained as a result of different molecular binding geometries, and the potential of having more than one wired molecule. As such factors can vary slightly from one experiment to another, this limits the degree to which peak positions can be compared. Hence, the observed 20% variation in the most probable conductance seen for each OPE3 compound is well within that naturally expected based on these factors alone. We conclude that any electronic effect of the DTF groups is less than this variation.

We find subtle differences between the results of the two setups including shorter 1 G_0 plateaus and fewer counts in the region immediately after the gold contact breakage for the MCBJ technique. The shorter 1 G_0 plateaus result in a less prominent peak in the histograms in Figure 5a−d. This is a known phenomenon related to the separation speed of the electrodes.[29] The rate of retraction in the STM was approximately 40 and 5 nms^{-1} in the MCBJ. Despite the shorter 1 G_0 plateaus, however, the stretching length of the molecules does not show the same consistent trend. This can be noticed in the 1D histograms in Figure 5a−d; the ratio of the molecular peak heights is much more similar than for the 1 G_0 peaks. This points to an insensitivity of the molecular junction lifetime within the range of retraction speeds tested. We have observed similar behavior in amine terminated OPEs.[30] It is also clear that more pure-tunneling traces are seen in the STM, and with greater counts in the region between $\log(G/G_0) = 0$ and −2. This may also be related to the speed of the measurement as the slower it is, the more the gold electrodes can retract through relaxation of the gold atoms.

We now focus on the other compounds for which a signal was found with the STM, but not for the MCBJ. This includes **7**, **15c**, and **10**. To highlight the differences, the 2D histograms built from only the traces containing plateaus are shown in Figure 6. We note that **15c** was previously studied by MCBJ[8f] using CH_2Cl_2 as solvent rather than dichlorobenzene. Under these conditions, a clear conductance plateau around 10^{-3} G_0 was seen, and it is likely the junctions here contains an aggregate of molecules. Calculations previously showed that the different *E*/*Z* isomers should have the same transmission at the Fermi level.[8d] A noticeable decrease in the conductance is found for **7** (amine anchors) (Figure 6e). The 1D histogram peak maximum is centered at $\log(G/G_0) = -4.6$ (2.5×10^{-5} G_0), almost 1 order of magnitude lower than for **6**. This value is consistent with previously reported values for amine terminated OPEs.[30] Between 8 and 20% of traces contained a conductance plateau depending on the experimental run, which is similar to **6**, but much lower than for the nonfunctionalized OPE diamine (50%).[30] This agrees with the results of **6**, supporting the observation that DTF units decrease junction formation probability.

Molecule **15c** (Figure 6f) gives a very weak signal, only 3% of traces showed a significant plateau. The low success rate in the break-junction experiment is once again consistent with the presence of a large amount of sulfur hindering the diffusion of the molecule into the junction. The plateau length is not, however, significantly longer than that observed for molecules **1**, **3**, **4**, **6**−**9**, despite the longest S−S distance in the molecule (2.9 nm), which is 0.8 nm more than in **1**, **3**, **4**, **6**−9. The 1D histogram peak is centered at $\log(G/G_0) = -4.6$, which is similar to **7** and suggests that rather than binding at the terminal S atoms, the molecule possibly adopts a configuration in which it binds through the face of a DTF unit to each electrode. This would explain both the shorter than expected plateaus and reasonably high conductance. For alternative binding scenarios (and calculated S−S distances), see SI.

In comparison, for OPE5 **10** (Figure 6g) we find a high rate of junction formation (similar to OPE3 **1**). In one experimental run we found a rate of 24%, which is higher by at least a factor of 2 compared to all the runs with the shorter exTTF-containing OPEs. A likely reason is that the greater flexibility of the long OPE5 prevents the DTFs from interacting strongly with gold. The conductance of **10** is significantly lower than that of **6**, with the peak in the 1D histogram centered at $\log(G/G_0) = -6.1$. This is consistent with a previous report of an OPE5[2f] and suggests the molecules indeed bind through their terminal S atoms. The mean plateau length of 2.1 nm is also consistent with the molecule binding in this way (adding the gold retraction results in a real spacing of 2.5−2.7 nm, and the calculated S−S distance is 3.3 nm).

Taking the conductance of **1** and **2** we can extract a β-value, which represents the degree of electronic attenuation of the OPE series under the present conditions. This yields a value of 3.7 nm^{-1}, close to the 3.4 nm^{-1} found by Kaliginedi et al.[31] for similar OPE molecules. We also find the same value for molecules **6** and **10** with the exTTF groups. This is, however, almost twice that of the 2 nm^{-1} found by photoinduced charge-transfer studies of TTF-OPE-C_{60} triads.[32] The lower β-value of the donor-bridge-acceptor system may be a result of the different tunnel-barrier heights in both systems, determined by the gold electrodes and donor/acceptor units, respectively.[33] In a study of OPE wires in a large-area junction device a still lower β-value of 1.5 nm^{-1} was found. In this study, Valkenier et al.[26] used gold electrodes, with a layer of PEDOT:PSS placed between the OPE layer and the top gold contact. Plausibly, the origin of the low value here could lie in the uncertainty in

dx.doi.org/10.1021/ja509937k | J. Am. Chem. Soc. 2014, 136, 16497−16507

Table 3. Summary of Conductances[a]

compound	DTFs [x.y]	greatest S−S distance (nm)	CP-AFM conductance (nS)	STM-BJ conductance (nS)	STM-BJ conductance, log(G/G_0) max
OPE3 **1**	[0.0]	2.0	1.49 ± 0.48	5.1 ± 0.05	−3.82 ± 0.44
OPE5 **2**	[0.0]	3.4	0.58 ± 0.35	0.062 ± 0.0003	−6.03 ± 0.3
OPE3 **3**	[0.1]	2.0	2.85 ± 2.23	4.0 ± 0.2	−3.85 ± 0.5
OPE3 **6**	[0.2]	2.0	5.56 ± 2.81	2.7 ± 0.5	−3.80 ± 0.64
OPE3 **9**	[0.2]	2.0	3.61 ± 2.75	10.6 ± 0.14	−3.74 ± 0.56
OPE5 **10**	[0.2]	3.4	2.28 ± 1.53	0.039 ± 0.0006	−6.14 ± 0.41
OPE3 **15**	[2.2]	3.4	4.06 ± 1.23 (**15d**)	0.74 ± 0.03 (**15c**)	−4.54 ± 0.67 (**15c**)

[a]For the CP-AFM data the conductance is the mean value, and the error is the standard deviation. For the STM-BJ we quote both (1) the maximum of the linear histogram representation, where the error is the error in the fit to a single Gaussian, and (2) the maximum in the log histogram (also fitted with a Gaussian), where the error is half the width at half-maximum. The peak maxima for **1**, **3**, **6**, and **9** remain approximately identical in the log(G/G_0) histogram but drop slightly in the linear histograms. The reason for this is the broadening, which occurs to both higher and lower values, can be seen in Figure S2 (SI) in the log histograms. This naturally shifts the linear maximum down but fails to capture the nature of the broadening. Hence, for the comparison of molecules using the BJ method, we prefer the log representation.

packing density of molecules in the junction and the thickness of the layer. It is also possible that the formation of a layer shifts the frontier orbitals relative to the isolated molecule case due to a difference in the polarizability of the environment,[34] for which there is also evidence in single-molecule junctions.[35]

The fact that we find essentially the same conductances and β-values for our exTTF molecules (**6** and **10**) as for the respective analogues without DTF groups (**1** and **2**) shows there is little influence of substitution, at least in the low bias regime, toward transport across single molecules in BJ experiments. Without further analysis, it is difficult to pin down the precise reasons for this, however it is possible that the orbitals responsible for transport have a low contribution from the DTF groups. Despite the fact that the DTF units are expected to contribute strongly to the HOMO, the main transport orbital is not necessarily this orbital. Transport could in fact be dominated by a lower lying level, such as the HOMO−2, which may be more delocalized through the molecule, providing better electronic coupling between the two electrodes.

The lower conductance found for the SAM in the OPE3 series (except for **6**) compared to the BJ measurements (see summary in Table 3) seems at first counterintuitive considering the high number of molecules expected to be present in each CP-AFM junction. This can, however, be convincingly explained by assuming that the top SAc remains intact in the SAM, while both SAc groups are likely cleaved in the BJ.[28] This would not only break the chemical contact of a Au−S direct bond but would also increase the length of the junction by the additional nonconjugated acetyl group at the interface to the Au tip.

A further interesting result of our study is the different trends seen for the same OPE3 backbone (**1**, **3**, **6**) with different numbers of DTF side groups between CP-AFM and BJ. The trend in the CP-AFM data follows the order $G_6 > G_3 > G_1$, while the BJ data show the molecules to have essentially the same conductance. To explain this we refer to the nature of the top contact in the CP-AFM. The probable lack of a covalent bond between the tip and the molecules could conceivably change the transport pathway through the layer. In the BJ, the main pathway most likely occurs through the entire molecule, from sulfur to sulfur. In the CP-AFM, the poorer top contact, combined with the known tilt of thiol monolayers, may force the current to take an alternative path. The poorer contact will decrease through-bond tunneling and increase through-space or intermolecule pathways. In the CP-AFM device geometry, which is a "push down" process with the tip load on top of the SAMs, a group of molecules is measured in the junctions; with the molecules being slightly tilted under the push (load force) from the CP-AFM tip. The tilt actually places the center of the molecule closer to the electrodes, so its influence on the charge transport would be greater than in the BJ measurement. We also note that this result is unlikely to be related to the total number of molecules in the junction as the DTFs contain reasonably bulky ester groups that should actually slightly reduce the density and, hence, the conductance of the layer. Based on this alone, there would have to be 3−4 times the density of molecules of **6** compared to **1** to explain the larger conductance. This seems physically unrealistic, supporting an explanation based on the transport pathway through the molecules. In the SAM molecular junctions, the molecular backbones are densely enough packed, such that the total current density could also contain contributions from both intramolecular (through-bond tunneling) and intermolecular (wire-to-wire tunneling) transport. We suggest that the combination of greater proximity of the central groups to the electrode, poorer top contact, and the greater likelihood of through-space or intermolecular transport pathways can account for the different conductance trend found for the SAM-based measurement compared to the single molecule result.

Overall, the comparison suggests that molecules can show different properties depending on their environment. Based on the conductance trend found by CP-AFM for **1**, **3** and **6**, we can assume that transport is dominated by the molecular HOMOs. On the other hand, the BJ results show no such trend, and this suggests that the HOMOs do not contribute significantly to the transport along the backbone. The upshot of this is that one technique alone cannot be used to predict the properties of molecular junctions in all environments. This has important consequences for the field of molecular electronics, where it has generally been assumed that studying the conductance at the fundamental level of just one molecule is useful for explaining the properties of larger molecular ensembles. Our work shows this particular concept may not be universally valid. Further studies are needed on a wider range of molecules to determine the extent of how electrical properties do or do not translate from the single- to the many-molecule case.

dx.doi.org/10.1021/ja509937k | J. Am. Chem. Soc. 2014, 136, 16497−16507

CONCLUSIONS

By a combination of Sonogashira, Wittig, and phosphite-mediated reactions, a large selection of cruciform-like OPE-TTF molecules was prepared. Thioacetate electrode anchoring groups were incorporated either as OPE end groups or as peripheral substituents on DTF termini. CP-AFM measurements on SAMs showed the conductance to increase with (1) decreasing length of the molecule, (2) an increasing number of orthogonally placed DTFs along the wire, and (3) by replacing aryl units of the OPE by DTFs. In contrast, both STM-BJ and MCBJ single-molecule measurements did not show any significant change in conductance by having DTFs along the OPE. Instead, the probability of trapping a molecule decreased systematically with the number of orthogonally placed DTFs within the OPE3 series (**1**, **3**, **6**); these probably offer alternative binding sites, reducing the mobility of the molecules for diffusing toward the junction. Despite this, the mean junction separation at breakdown was virtually identical across this series, indicating that within the junction the DTFs do not cause significant instability. Notably, measurements on SAMs provide significantly lower conductances than those on single molecules. One reasonable explanation is the different connecting geometries of the device. In the CP-AFM measurements on SAMs, we most likely have a junction structure corresponding to Au−S−OPE−SAc ||| Au, where the top sulfur is not covalently linked to Au (indicated by ||| symbol), while the BJs in most cases likely correspond to Au−S−OPE−S−Au (covalent anchoring to both electrodes). The lack of a covalent top linkage may be responsible for the different trends seen for the single-molecule and SAM studies by altering the conductance pathway across the junction. The different outcome not only brings to the forefront the challenge of characterizing conducting properties of complex molecules containing several sulfur atoms as potential binding sites but also stresses the importance of the interface with regard to the observed trends within series of molecules. It is very gratifying that CP-AFM/SAM studies carried out in different laboratories (Beijing/Au tip vs Copenhagen/Pt tip (previous work)) reveal similar trends as do BJ studies carried out in different laboratories (Madrid/STM-BJ vs Delft/MCBJ).

ASSOCIATED CONTENT

Supporting Information

Experimental procedures, characterization data, and NMR spectra. This material is available free of charge via the Internet at http://pubs.acs.org.

AUTHOR INFORMATION

Corresponding Authors

edmund.leary@imdea.org
zmwei@iccas.ac.cn
H.S.J.vanderZant@tudelft.nl
mbn@kiku.dk.

Notes

The authors declare no competing financial interest.

ACKNOWLEDGMENTS

The European Union seventh Framework Programme (FP7/2007-2013) under the grant agreement no. 270369 ("ELFOS"), University of Copenhagen, FOM, NWO/OCW, ERC (advanced ERC grant), (Mols@Mols), "MOLESCO" (Project number 606728), and Spanish MICINN/MINECO through the programs MAT2011-25046 are thanked for support.

REFERENCES

(1) (a) Robertson, N.; McGowan, C. A. *Chem. Soc. Rev.* **2003**, *32*, 96−103. (b) Benniston, A. C. *Chem. Soc. Rev.* **2004**, *33*, 573−578. (c) Nørgaard, K.; Bjørnholm, T. *Chem. Commun.* **2005**, 1812−1823. (d) Weibel, N.; Grunder, S.; Mayor, M. *Org. Biomol. Chem.* **2007**, *5*, 2343−2353. (e) Klajn, R.; Stoddart, J. F.; Grzybowski, B. A. *Chem. Soc. Rev.* **2010**, *39*, 2203−2237.

(2) (a) Tour, J. M.; Rawlett, A. M.; Kozaki, M.; Yao, Y.; Jagessar, R. C.; Dirk, S. M.; Price, D. W.; Reed, M. A.; Zhou, C.-W.; Chen, J.; Wang, W.; Campbell, I. *Chem.—Eur. J.* **2001**, *7*, 5118−5134. (b) Mayor, M.; Weber, H. B.; Reichert, J.; Elbing, M.; von Hänisch, C.; Beckmann, D.; Fischer, M. *Angew. Chem., Int. Ed.* **2003**, *42*, 5834−5838. (c) Huber, R.; González, M. T.; Wu, S.; Langer, M.; Grunder, S.; Horhoiu, V.; Mayor, M.; Bryce, M. R.; Wang, C.; Jichati, R.; Schönenberger, C.; Calame, M. *J. Am. Chem. Soc.* **2008**, *130*, 1080−1084. (d) Vonlanthen, D.; Mishchenko, A.; Elbing, M.; Neuburger, M.; Wandlowski, T.; Mayor, M. *Angew. Chem., Int. Ed.* **2009**, *48*, 8886−8890. (e) Kaliginedi, V.; Moreno-García, P.; Valkenier, H.; Hong, W.; García-Suárez, V. M.; Buiter, P.; Otten, J. L. H.; Hummelen, J. C.; Lambert, C. J.; Wandlowski, T. *J. Am. Chem. Soc.* **2012**, *134*, 5262−5275. (f) Frisenda, R.; Perrin, M. L.; Valkenier, H.; Hummelen, J. C.; van der Zant, H. S. J. *Phys. Status Solidi B* **2013**, *250*, 2431−2436.

(3) Aviram, A.; Ratner, M. A. *Chem. Phys. Lett.* **1974**, *29*, 277−283.

(4) (a) Segura, J. L.; Martín, N. *Angew. Chem., Int. Ed.* **2001**, *40*, 1372−1409. (b) Perepichka, D. F.; Bryce, M. R.; Pearson, C.; Petty, M. C.; McInnes, E. J. L.; Zhao, J. P. *Angew. Chem., Int. Ed.* **2003**, *42*, 4636−4639. (c) Ho, G.; Heath, J. R.; Kondratenko, M.; Perepichka, D. F.; Arseneault, K.; Pézolet, M.; Bryce, M. R. *Chem.—Eur. J.* **2005**, *11*, 2914−2922. (d) Leroy-Lhez, S.; Baffreau, J.; Perrin, L.; Levillain, E.; Allain, M.; Blesa, M.-J.; Hudhomme, P. *J. Org. Chem.* **2005**, *70*, 6313−6320.

(5) (a) Lou, Y.; Collier, P.; Jeppesen, J. O.; Nielsen, K. A.; Delonno, E.; Ho, G.; Perkins, J.; Tseng, H.-R.; Yamamoto, T.; Stoddart, J. F.; Heath, J. R. *ChemPhysChem* **2002**, *3*, 519−525. (b) Giacalone, F.; Herranz, M.; Grüter, L.; González, M. T.; Calame, M.; Schönenberger, C.; Arroyo, C. R.; Rubio-Bollinger, G.; Vêlez, M.; Agraït, N.; Martín, N. *Chem. Commun.* **2007**, 4854−4856. (c) Leary, E.; Higgins, S. J.; van Zalinge, H.; Haiss, W.; Nichols, R. J.; Nygaard, S.; Jeppesen, J. O.; Ulstrup, J. *J. Am. Chem. Soc.* **2008**, *130*, 12204−12205. (d) Liao, J.; Agustsson, J. S.; Wu, S.; Schönenberger, C.; Calame, M.; Leroux, Y.; Mayor, M.; Jeannin, O.; Ran, Y.-F.; Liu, S.-X. *Nano Lett.* **2010**, *10*, 759−764.

(6) (a) Love, J. C.; Estroff, L. A.; Kriebel, J. K.; Nuzzo, R. G.; Whitesides, G. M. *Chem. Rev.* **2005**, *105*, 1103−1169. (b) Stuhr-Hansen, N.; Sørensen, J. K.; Moth-Poulsen, K.; Christensen, J. B.; Bjørnholm, T.; Nielsen, M. B. *Tetrahedron* **2005**, *61*, 12288−12295. (c) Nørgaard, K.; Nielsen, M. B.; Bjørnholm, T. In *Functional Organic Materials*; Müller, T. J. J., Bunz, U. H. F., Eds.; Wiley-VCH: Weinheim, Germany, 2007; pp 353−392.

(7) (a) Nuzzo, R. G.; Allara, D. L. *J. Am. Chem. Soc.* **1983**, *105*, 4481−4483. (b) Strong, L.; Whitesides, G. M. *Langmuir* **1988**, *4*, 546−558. (c) Kubatkin, S.; Danilov, A.; Hjort, M.; Cornil, J.; Brédas, J.-L.; Stuhr-Hansen, N.; Hedegård, P.; Bjørnholm, T. *Nature* **2003**, *425*, 698−701. (d) Love, J. C.; Estroff, L. A.; Kriebel, J. K.; Nuzzo, R. G.; Whitesides, G. M. *Chem. Rev.* **2005**, *105*, 1103−1169. (e) Meisner, J. S.; Ahn, S.; Aradhya, S. V.; Krikorian, M.; Parameswaran, R.; Steigerwald, M.; Venkataraman, L.; Nuckolls, C. *J. Am. Chem. Soc.* **2012**, *134*, 20440−20445.

(8) (a) Sørensen, J. K.; Vestergaard, M.; Kadziola, A.; Kilså, K.; Nielsen, M. B. *Org. Lett.* **2006**, *8*, 1173−1176. (b) Jennum, K.; Vestergaard, M.; Pedersen, A. H.; Fock, J.; Jensen, J.; Santella, M.; Led, J. J.; Kilså, K.; Bjørnholm, T.; Nielsen, M. B. *Synthesis* **2011**, 539−548. (c) Wei, Z.; Li, T.; Jennum, K.; Santella, M.; Bovet, N.; Hu, W.; Nielsen, M. B.; Bjørnholm, T.; Solomon, G. C.; Laursen, B. W.; Nørgaard, K. *Langmuir* **2012**, *28*, 4016−4023. (d) Parker, C. R.; Wei, Z.; Arroyo, C. R.; Jennum, K.; Li, T.; Santella, M.; Bovet, N.; Zhao, G.;

Hu, W.; van der Zant, H. S. J.; Vanin, M.; Solomon, G. S.; Laursen, B. W.; Nørgaard, K.; Nielsen, M. B. *Adv. Mater.* **2013**, *25*, 405−409. (e) Fock, J.; Leijnse, M.; Jennum, K.; Zyazin, A. S.; Paaske, J.; Hedegård, P.; Nielsen, M. B.; van der Zant, H. S. J. *Phys. Rev. B* **2012**, *86*, 235403. (f) Schou, S. S.; Parker, C. R.; Lincke, K.; Jennum, K.; Vibenholt, J.; Kadziola, A.; Nielsen, M. B. *Synlett* **2013**, *24*, 231−235.
(9) See for example: Zucchero, A. J.; McGrier, P. L.; Bunz, U. H. F. *Acc. Chem. Res.* **2010**, *43*, 397−408.
(10) Andersson, A. S.; Qvortrup, K.; Torbensen, E. R.; Mayer, J.-P.; Gisselbrecht, J.-P.; Boudon, C.; Gross, M.; Kadziola, A.; Kilså, K.; Nielsen, M. B. *Eur. J. Org. Chem.* **2005**, 3660−3671.
(11) Sonogashira, K.; Tohda, Y.; Hagihara, N. *Tetrahedron Lett.* **1975**, *16*, 4467−4470.
(12) CO_2Me analogue of **16** − known compound: Zhang, Q.; Shi, C.; Zhang, H.-R.; Wang, K. K. *J. Org. Chem.* **2000**, *65*, 7977−7983.
(13) CO_2Me analogue of **18** − known compound: Jacobsen, M. F.; Ravnsbæk, J. B.; Gothelf, K. V. *Org. Biomol. Chem.* **2010**, *8*, 50−52.
(14) Wang, L.-G.; Zhan, T.-G.; Zhao, X.; Jiang, X.-K.; Li, Z.-T. *Tetrahedron* **2012**, *68*, 5303−5310.
(15) Cade, I.; Long, N. J.; White, A. J. P.; Williams, D. J. *J. Organomet. Chem.* **2006**, *691*, 1389−1401.
(16) Sato, M.; Gonnella, N. C.; Cava, M. P. *J. Org. Chem.* **1979**, *44*, 930−933.
(17) (a) Baxendale, I. R.; Schou, S. C.; Sedelmeier, J.; Ley, S. V. *Chem.—Eur. J.* **2010**, *16*, 89−94. (b) Egi, M.; Azechi, K.; Saneto, M.; Shimizu, K.; Akai, S. *J. Org. Chem.* **2010**, *75*, 2123−2126.
(18) Hu, L.-Y.; Ryder, T. R.; Rafferty, M. F.; Taylor, C. P.; Feng, M. R.; Kuo, B.-S.; Lotarski, S. M.; Miljanich, G. P.; Millerman, E.; Siebers, K. M.; Szoke, B. G. *Bioorg. Med. Chem.* **2000**, *8*, 1203−1212.
(19) Baffreau, J.; Dumur, F.; Hudhomme, P. *Org. Lett.* **2006**, *8*, 1307−1310.
(20) (a) Wadsworth, W. S., Jr. *Org. React.* **1977**, *25*, 73−253. (b) Maryanoff, B. E.; Reitz, A. B. *Chem. Rev.* **1989**, *89*, 863−927.
(21) Crystal data for **50**: $C_{34}H_{38}O_8S_4Si_2$, M_r = 759.11, orthorhombic, *Pbca*, a = 20.3534(10), b = 8.3596(5), c = 22.6457(11), V = 3853.1(4), T = 122(1) K, $\mu(Mo_{K\alpha})$ = 0.355, $2\theta_{max}$= 53.46°, 49188 reflections measured, 4097 unique reflections (R_{int} = 0.1405), $R1(I > 4\sigma(I))$ = 0.0426, *wR2*(all data) = 0.0981, S = 1.043. CCDC 1005219 contains the supplementary crystallographic data for this paper. These data can be obtained free of charge from The Cambridge Crystallographic Data Centre via www.ccdc.cam.ac.uk/data_request/cif.
(22) Mulla, K.; Zhao, Y. *J. Mater. Chem. C* **2013**, *1*, 5116−5127.
(23) Svenstrup, N.; Rasmussen, K. M.; Hansen, T. K.; Becher, J. *Synthesis* **1994**, 809−812.
(24) Simonsen, K. B.; Svenstrup, N.; Lau, J.; Simonsen, O.; Mørk, P.; Kristensen, G. J.; Becher, J. *Synthesis* **1996**, 407−418.
(25) (a) Sallé, M.; Belyasmine, A.; Gorgues, A.; Jubault, M.; Soyer, N. *Tetrahedron Lett.* **1991**, *32*, 2897−2900. (b) Lorcy, D.; Carlier, R.; Robert, A.; Tallec, A.; Le Maguerès, P.; Ouahab, L. *J. Org. Chem.* **1995**, *60*, 2443−2447. (c) Frère, P.; Skabara, P. J. *Chem. Soc. Rev.* **2005**, *34*, 69−98.
(26) Valkenier, H.; Huisman, E. H.; van Hal, P. A.; de Leeuw, D. M.; Chiechi, R. C.; Hummelen, J. C. *J. Am. Chem. Soc.* **2011**, *133*, 4930−4939.
(27) (a) Choi, S. H.; Kim, B.; Frisbie, C. D. *Science* **2008**, *320*, 1482−1486. (b) Guédon, C. M.; Valkenier, H.; Markussen, T.; Thygesen, K. S.; Hummelen, J. C.; van der Molen, S. J. *Nat. Nanotechnol.* **2012**, *7*, 305−309.
(28) González, M. T.; Leary, E.; García, R.; Verma, P.; Herranz, M. Á.; Rubio-Bollinger, G.; Martín, N.; Agraït, N. *J. Phys. Chem. C* **2011**, *115*, 17973−17978.
(29) Tsutsui, M.; Shoji, K.; Taniguchi, M.; Kawai, T. *Nano Lett.* **2008**, *8*, 345−349.
(30) González, M. T.; Díaz, A.; Leary, E.; García, R.; Herranz, M. Á.; Rubio-Bollinger, G.; Martín, N.; Agraït, N. J. *Am. Chem. Soc.* **2013**, *135*, 5420−5426.
(31) Kaliginedi, V.; Moreno-García, P.; Valkenier, H.; Hong, W.; García-Suárex, V. M.; Buiter, P.; Hotten, J. L. H.; Hummelen, J. C.; Lamert, C. J.; Wandlowski, T. *J. Am. Chem. Soc.* **2012**, *134*, 5262−5275.
(32) Atienza, C.; Martín, N.; Wielopolski, M.; Haworth, N.; Clark, T.; Guldi, D. M. *Chem. Commun.* **2006**, 3202−3204.
(33) Adams, D. M.; Brus, L.; Chidsey, C. E. D.; Creager, S.; Creutz, C.; Kagan, C. R.; Kamat, P. V.; Lieberman, M.; Lindsay, S.; Marcus, R. A.; Metzger, R. M.; Michel-Beyerle, M. E.; Miller, J. R.; Newton, M. D.; Rolison, D. R.; Sankey, O.; Schanze, K. S.; Yardley, J.; Zhu, X. *J. Phys. Chem. B* **2003**, *107*, 6668−6697.
(34) Torrente, I. F.; Franke, K. J.; Pacual, J. I. *J. Phys.: Condens. Matter* **2008**, *20*, 184001.
(35) Leary, E.; Höbenreich, H. H.; Higgins, S. J.; van Zalinge, H.; Haiss, W.; Nichols, R. J.; Finch, C. M.; Grace, I.; Lambert, C. J.; McGrath, R.; Smerdon, J. *Phys. Rev. Lett.* **2009**, *102*, 086801.